PROCEEDINGS OF SPIE

SPIEDigitalLibrary.org/conference-proceedings-of-spie

Investigation of low-n mask in 0.33 NA EUV single patterning at pitch 28nm metal design

Dongbo Xu, Werner Gillijns, Ling Ee Tan, Vicky Philipsen, Ryoung-Han Kim

Dongbo Xu, Werner Gillijns, Ling Ee Tan, Vicky Philipsen, Ryoung-Han Kim, "Investigation of low-n mask in 0.33 NA EUV single patterning at pitch 28nm metal design," Proc. SPIE 12051, Optical and EUV Nanolithography XXXV, 120510H (26 May 2022); doi: 10.1117/12.2614197

SPIE.

Event: SPIE Advanced Lithography + Patterning, 2022, San Jose, California, United States

Downloaded From: https://www.spiedigitallibrary.org/conference-proceedings-of-spie on 19 Sep 2022 Terms of Use: https://www.spiedigitallibrary.org/terms-of-use

Investigation of Low-n Mask in 0.33NA EUV Single Patterning at Pitch 28nm Metal Design

Dongbo Xu, Werner Gillijns, Ling Ee Tan, Vicky Philipsen, Ryoung-han Kim

imec, Kapeldreef 75, 3001 Leuven, Belgium

ABSTRACT

Extending 0.33NA EUV single patterning to 28nm pitch becomes very challenging in terms of stochastic defectivity, which demands high contrast lithographic images. The low-n attenuated phase-shift mask (attPSM) can provide superior solutions for individual pitches by mitigating mask three-dimensional effects. The simulation and experiment results have shown substantial imaging improvements: higher depth of focus at similar normalized image log slope and smaller telecentricity error values than the best binary mask configuration. In this paper, the exploration of low-n attPSM patterning opportunity for pitch 28nm metal design is investigated. The lithographic performance of the low-n attPSM is compared to the standard binary Ta-based absorber mask. As well, the impact of mask tonality (bright-field vs. dark-field) on the pattern fidelity and process window is evaluated both by simulations and experiments.

Keywords: EUV Single Patterning, Phase-shift Mask, Low-n, Pitch 28nm

1. INTRODUCTION

Nowadays, extreme ultraviolet lithography (EUVL) has been part of high-volume manufacturing (HVM). To further push 0.33NA EUV single patterning down to pitch 28nm metal design becomes very challenging in terms of stochastic defectivity and process window. It is requiring complex and expensive design, mask and process co-optimization. Currently, imec is developing and evaluating the patterning techniques to enable 0.33NA EUV single patterning at pitch 28nm.[1–4] To have a good control of stochastic variability at tight pitch, high Normalized Image Log-Slope (NILS) is required. However, Mask three-Dimensional (M3D) effects have been well known in EUVL imaging, which introduces lithographic image contrast fading, telecentricity errors through focus, best focus shift through pitch and through slit printability issues.[5–8] To mitigate the M3D effects, one approach is to employ alternative mask stacks.[7,9–17] The low-n attenuated phase-shift mask (attPSM) has shown substantial imaging improvements both in simulations and experiments: higher depth of focus (DoF) at similar NILS and smaller telecentricity errors than the best binary mask configuration.[13,18–20] In this paper, the exploration of using low-n attPSM for patterning pitch 28nm metal design is investigated both by simulations and experiments, the impact of mask tonality is considered as well. To have a straightforward comparison, the standard binary Ta-based absorber masks (dark- and bright-field) are used as the references. The lithographic performance of the low-n attPSM for patterning pitch 28nm metal design is evaluated using the first imec low-n attPSM masks (dark- and bright-field masks).

The paper is organized as follows. Section 2 gives the context. The Source Mask Optimization (SMO) strategy and the Mask Optimization (MO) results using the given low-n attPSM stack information will be briefly introduced. Section 3 compares the lithographic patterning performance between the low-n attPSM and the reference binary mask by simulations and experiments, for patterning vertical pitch 28nm metal design based on generic building blocks. The last section will provide the summary.

Further author information: Dongbo Xu; E-mail: dongbo.xu@imec.be, Telephone: +32 16 28 35 77

Optical and EUV Nanolithography XXXV, edited by Anna Lio, Martin Burkhardt, Proc. of SPIE Vol. 12051, 120510H · © 2022 SPIE · 0277-786X · doi: 10.1117/12.2614197

Downloaded From: https://www.spiedigitallibrary.org/conference-proceedings-of-spie on 19 Sep 2022
Terms of Use: https://www.spiedigitallibrary.org/terms-of-use

2. CONTEXT

In this paper, the simulations and experiments of the use-case are performed at conditions of imec's 0.33NA NXE:3400 EUV scanner.[21] The same SMO strategy in the paper of Xu et al.[17] was carried out together with the actual low-n attPSM stack provided by the maskshop, to obtain the optimized source for the low-n attPSM.

Figure 1 shows the optimized sources respective for binary mask and low-n attPSM, the SMO input target clip is vertical pitch 28nm 1:1 Line/Space grating. These two sources are very similar with minor difference and will be used for all the simulations and experiments, for dark-field and bright-field of both low-n attPSMs and binary masks.

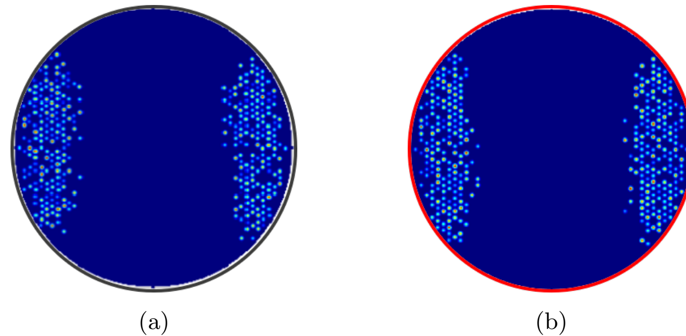

Figure 1: SMO optimized sources when using vertical pitch 28nm Line/Space grating as the input target: (a) source for the reference binary mask; (b) source for the low-n attPSM.

Figure 2 shows the imec N3 random logic design clip that is used in the MO steps, the process window evaluation points are placed as the red cutlines across the $1\mu\text{m}^2$ design area. Our previous investigation demonstrates that the low-n attPSM performs the best for 0.33NA EUV single patterning at pitch 28nm, both for dark-field mask with sub-resolution assist features (SRAFs) and bright-field mask without SRAFs.[17]

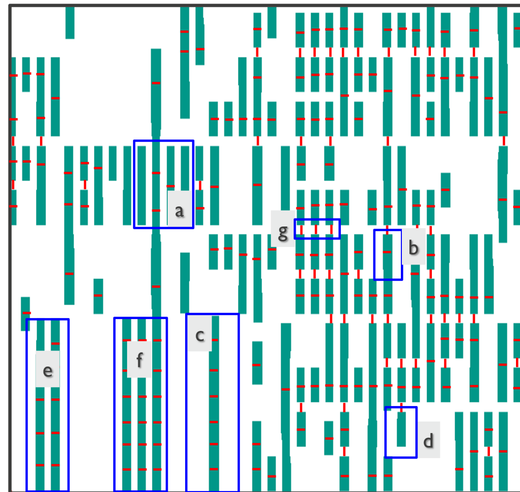

Figure 2: imec N3 random logic design clip with design retargeting: (a) dense Line/Space, the minimum pitch is 28nm, and the minimum trench CD is 14nm; (b) and (d) semi-dense features; (c) isolated feature; (e) Two-Bar; (f) Three-Bar; (g) T2T with CD is 20nm. Semi-isolated and isolated features target CD are between 14nm and 18nm. The red cutlines are used for OPW evaluation.

Figure 3 shows the exposure latitude (EL) vs. DoF of CD-based overall process window (OPW) both for dark-field mask with SRAFs and bright-field mask without SRAFs. An example of OPW is shown on the top

Downloaded From: https://www.spiedigitallibrary.org/conference-proceedings-of-spie on 19 Sep 2022
Terms of Use: https://www.spiedigitallibrary.org/terms-of-use

right of the figure, which is calculated by overlapping the process window of each red cutline shown in Fig. 2, and the fitting ellipse is used to compute the overall EL and DoF. With respect to the reference dark-field binary mask, the dark-field low-n attPSM with SRAFs gains ∼40% overall EL; and the bright-field mask without SRAFs gains ∼25% overall EL compared to bright-field binary mask. In general, bright-field masks without SRAFs deliver smaller overall DoF with respect to the dark-field mask with SRAFs.

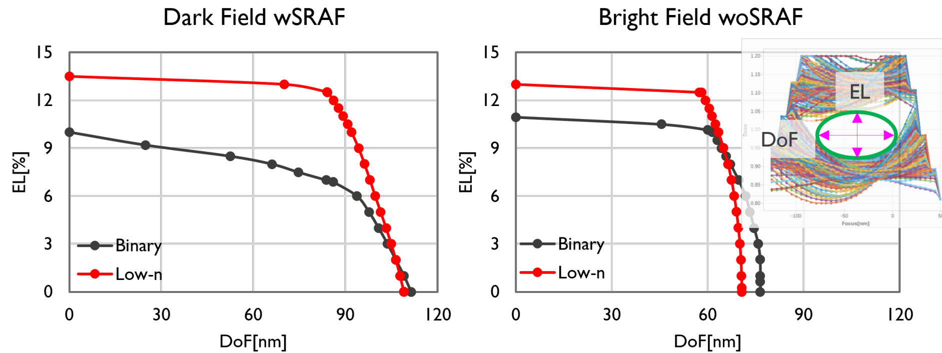

Figure 3: Exposure latitude (EL) vs. depth of focus (DoF) of CD-based overall process window (OPW) both for dark-field mask with SRAFs and bright-field mask without SRAFs. CD-based OPWs obtained with ± 10% CD tolerance on trenches, ±20% CD tolerance on T2Ts, the actual mask stack info is used.

3. LITHOGRAPHIC PERFORMANCE COMPARISON BETWEEN THE LOW-N ATTPSM AND THE BINARY MASK

The imec N3 random logic design clip shown in Fig. 2 can be decomposed into several generic building blocks, such as:

1. dense Line/Space, the minimum pitch and CD are 28nm and 14nm, respectively;
2. semi-dense and isolated Line/Space, the trench CDs are varying between 14nm and 18nm;
3. Two-Bar and Three-Bar geometries, the minimum target resist line CD between two bars is 14nm;
4. T2Ts, the minimum CD of T2T at pitch 28nm is 20nm.

Therefore, the patterning performance between the low-n attPSM and the reference binary mask is compared using these selected building blocks in this section: vertical Line/Space through pitch, Two-Bar at pitch 28nm, T2T at pitch 28nm with through target T2T CD. The side-lobe printing risk will be assessed using the edge of the build block of Line/Space at pitch 28nm.

3.1 Line/Space Through Pitch

a) Best Focus Shift

The EUV-inherent M3D effects introduce best focus shifts through pitch. Figure 4 compares the best focus shift through pitch of the low-n attPSMs and the reference binary masks. The left figure shows the simulation results, and the right figure presents the experimental results obtained from imec's 0.33NA NXE:3400 EUV scanner. The results demonstrate that the dark-field low-n attPSM has the largest best focus shifts through pitch, the isolated feature results in 140nm best focus shift with respect to the dense features. The bright-field low-n attPSM has much smaller best focus shifts with respect to the dark-field low-n attPSM, which is similar to the dark- and bright-field binary masks. Therefore, the bright-field low-n attPSM and the reference binary masks could deliver certain OPW without considering SRAFs, the OPWs of bright-field masks are shown in Fig. 3, more details of OPW comparisons are reported by Xu et. al.[17]

To mitigate the best focus shifts through pitch of dark-field low-n attPSM, design retargeting and SRAF insertion are typically considered. Figure 5 shows the best focus shifts through mask CD of Line/Space gratings

Downloaded From: https://www.spiedigitallibrary.org/conference-proceedings-of-spie on 19 Sep 2022
Terms of Use: https://www.spiedigitallibrary.org/terms-of-use

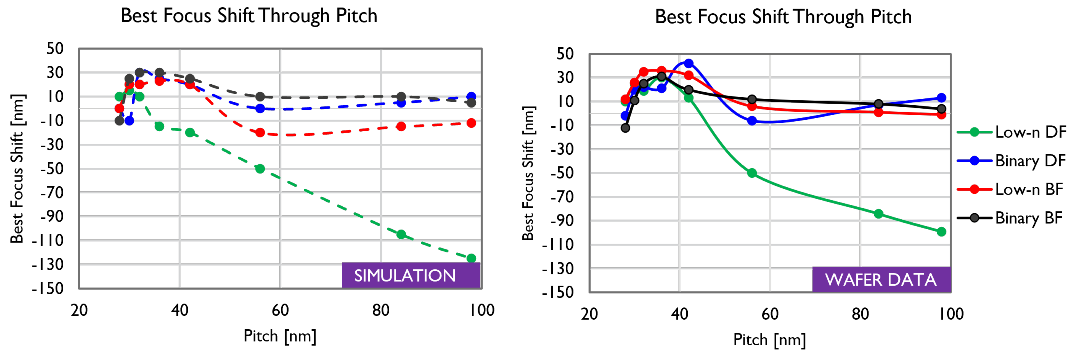

Figure 4: Best focus shifts through pitch of the low-n attPSM and the reference binary mask. DF: dark-field; BF: bright-field. The left figure shows the simulation results, and the right figure presents the experimental results obtained from NXE:3400. The sources are shown in Fig. 1.

at pitch 98nm. The left figure is the simulation result and the right figure is the wafer data. The big best focus shift of the dark-field low-n attPSM can be partly reduced by increasing the mask CD, and the minimum best focus shift ∼50nm occurs at mask CD around 32nm. However, as the mask CD becomes larger, the best focus shift becomes larger again. Therefore, only playing with the mask CD bias is not able to completely mitigate the best focus shift introduced by the dark-field low-n attPSM, SRAF insertion is required as well.

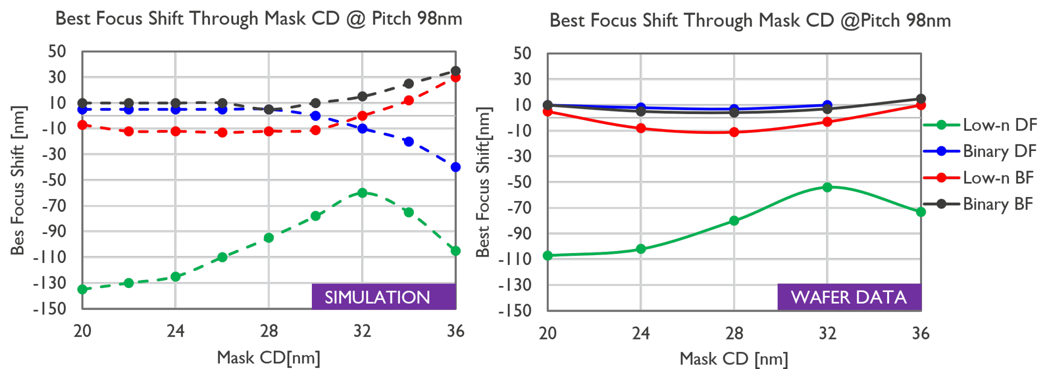

Figure 5: Best focus shifts through mask CD of Line/Space gratings at pitch 98nm. DF: dark-field; BF: bright-field. The left figure shows the simulation results, and the right figure presents the experimental results obtained from 0.33NA NXE:3400 EUV scanner. The sources are shown in Fig. 1.

Figure 6 shows the intensity profile distribution propagating through focus for Line/Space grating at pitch 56nm and mask CD 20nm. The best focus of each case is defined by the center of the corresponding OPW. Comparing the four use cases shown in the figure, because of large best focus shift through pitch of the dark-field low-n attPSM, the feature does not print at defocus =-50nm. When the intensity propagates further through focus, the simulation shows that the background intensity will exceed the model threshold and print on the wafer. It is due to the interference between the diffraction light and background light, Therefore, to mitigate the best focus shift of this feature by SRAF becomes very challenging.

Considering SRAF insertion of the dark-field mask, overexposure is required to evaluate the SRAF printing risk. Figure 7 shows the optical simulated relationship between overexposure latitude and SRAF CD at defocus in the range of -50nm and +50nm with step of 10nm. To avoid SRAF printing inside of the OPW, a certain EL through focus is needed. The top figure demonstrates that to have a reasonable EL through focus (>10%), SRAF CD needs to be smaller than 6nm, which is beyond current Mask Rules Check (MRC). Considering current MRC

Downloaded From: https://www.spiedigitallibrary.org/conference-proceedings-of-spie on 19 Sep 2022
Terms of Use: https://www.spiedigitallibrary.org/terms-of-use

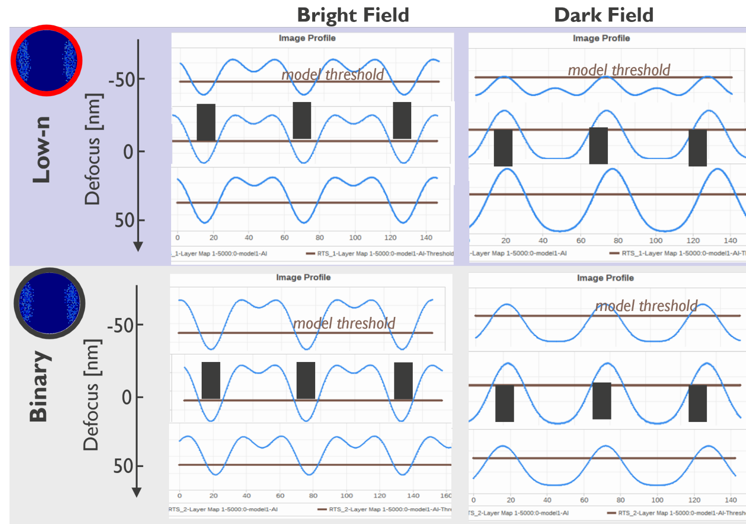

Figure 6: Aerial image intensity profile distribution through focus for Line/Space grating: pitch 56nm, mask CD 20nm. The best focus for each case is defined by the center of the corresponding OPW shown in Fig. 3.

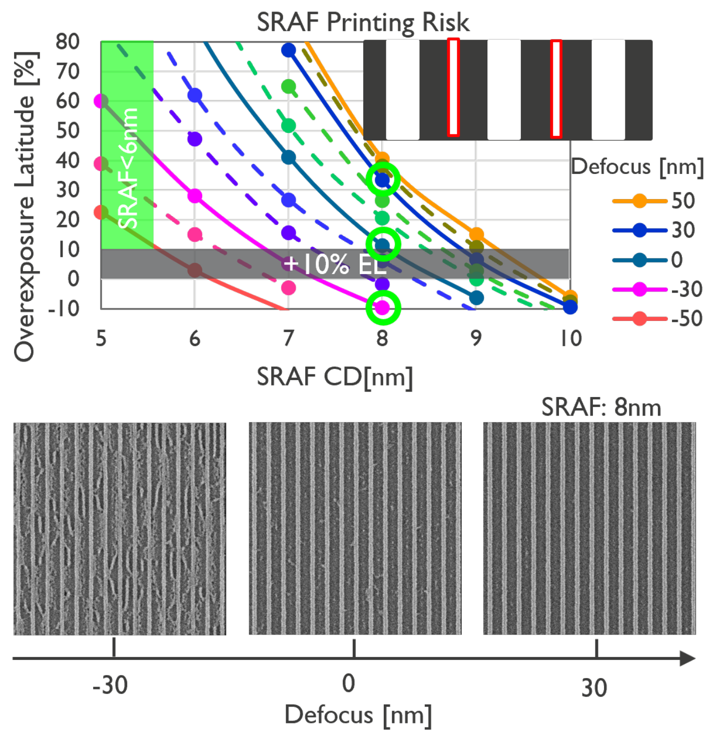

Figure 7: The relationship between overexposure latitude and SRAF CD for Line/Space grating: pitch 56nm, mask CD 20nm, the high lighted three points using the circle are the EL of 8nm SRAF at defocus -30nm, 0nm and +30nm.

of 8nm SRAF size, the high lighted points show that the overexposure latitude is $< 0\%$ and $> 30\%$ at -30nm and +30nm defocus, respectively. This means SRAF CD equal to 8nm will print on the wafer at -30nm defocus, but will not print at +30nm defocus with the nominal dose. The bottom figure presents the measured SEM

Downloaded From: https://www.spiedigitallibrary.org/conference-proceedings-of-spie on 19 Sep 2022
Terms of Use: https://www.spiedigitallibrary.org/terms-of-use

images of Line/Space pitch 56nm mask CD 20nm with 8nm SRAF size through focus, SRAF starts printing at best focus condition. Therefore, design retargeting is necessary for this feature.

b) NILS Distribution

Figure 8 shows the NILS distribution vs. pitch/mask CD, the purple line in the figure is the pattern density equal to 0.5, and the blue rectangle in the figure represents the pitch and mask CD distribution of the imec N3 pitch 28nm relevant design. The left column is the bright-field mask use case, the NILS distribution is mainly mask CD dependent. The bright-field low-n attPSM has slight better NILS for dense Line/Space with pitch <45nm, and has a slight severe forbidden pitch phenomena with respect to the bright-field binary mask. The bright-field binary mask has good NILS distribution through pitch (>40nm) with large mask CD (>20nm). To pattern the iN3 pitch 28nm relevant design, the bright-field low-n attPSM has slightly better NILS with smaller mask CD with respect to the binary mask.

The right column is the dark field mask use case. As shown in the figure, the mask tonality has a significantly impact on the NILS distribution, and the dark-field low-n attPSM and binary mask have similar NILS distribution through pitch and mask CD. The NILS distribution of the dark-field mask has a clear transition region at the density ~ 0.5. Dark-field mask with large CD and higher pattern density (>0.5) enables good NILS. There is a slight difference as the pitch and mask CD becomes larger. In general, for patterning the imec N3 pitch 28nm relevant design, dark-field masks have lower NILS through pitch and mask CD with respect to the bright-field masks.

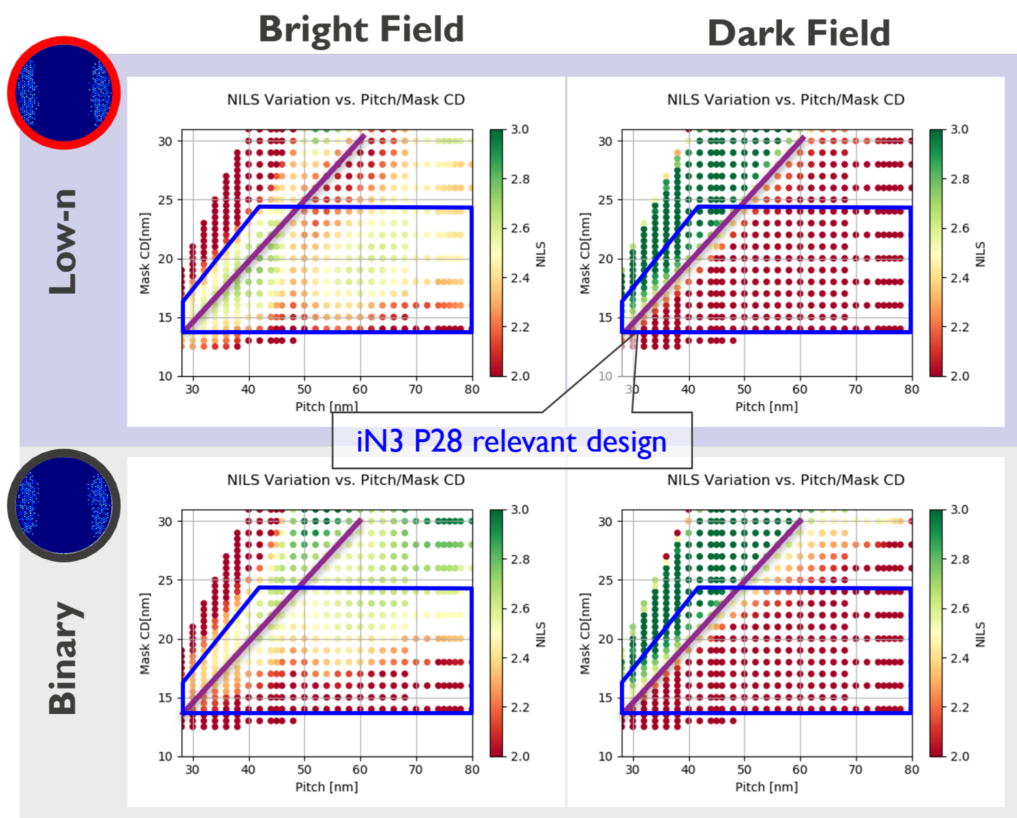

Figure 8: NILS distribution vs. Pitch/Mask CD. The blue rectangle is pitch and mask CD distribution of the iN3 relevant design pattern.

Considering the tightest pitch 28nm Line/Space grating, Fig. 9 displays the dose sensitivity and pattern printability of the bright-field masks comparison between low-n attPSM and the reference binary mask. The left figure is the dose sensitivity vs. the mask CD at pitch 28nm. The triangles are the current wafer anchors. The

Downloaded From: https://www.spiedigitallibrary.org/conference-proceedings-of-spie on 19 Sep 2022
Terms of Use: https://www.spiedigitallibrary.org/terms-of-use

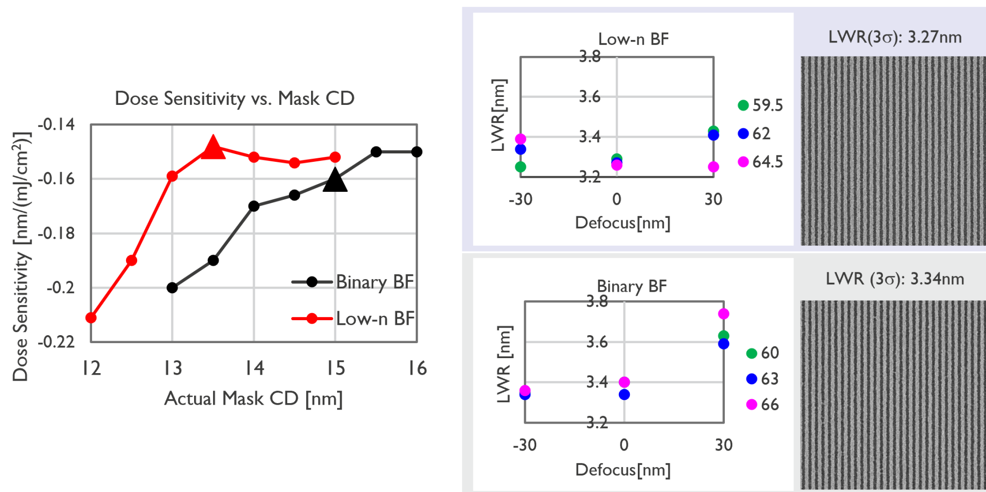

Figure 9: Dose sensitivity and pattern printability of the bright-field masks comparison between low-n attPSM bright-field mask and the reference binary bright-field mask, for patterning dense pitch 28nm Line/Space gratings, LWR is not measured by BKM, and only for comparison purpose.

bright-field mask of the low-n attPSM has a slightly lower dose sensitivity with respect to the binary mask. The right figures are the line width roughness (LWR) comparison, the bright-field low-n attPSM slightly improves the LWR with respect to the bright-field binary mask.

3.2 Two-Bar Printability

a) Two-Bar Pitch 28nm

Our study shows that one of the main hotspots for pitch 28nm random logic design patterning is the Two-Bar at pitch 28nm. The left figure of Fig. 10 is a design clip, and the high lighted position is the pitch 28nm Two-Bar design, where the vias are landing on top of the metals. The width of the design polygon (resist trench or metal) and the space (resist line) between two polygons are both 14nm. To have a good patterning quality, the two

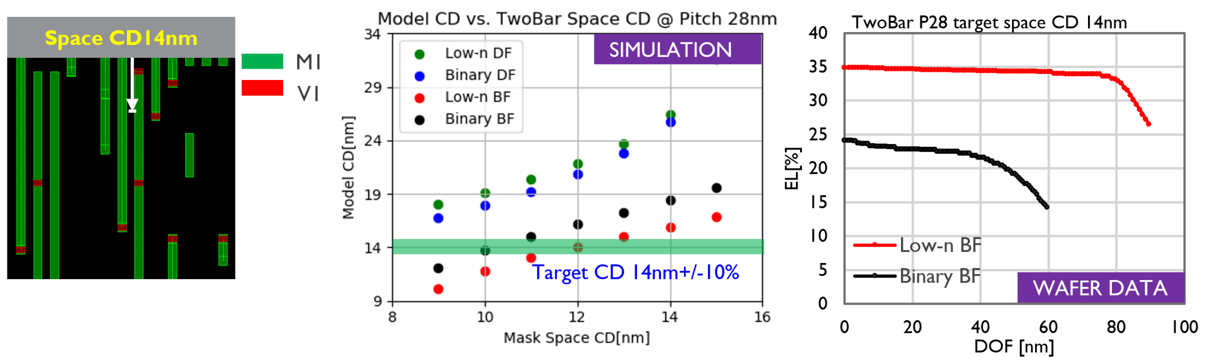

Figure 10: Two-Bar printability at pitch 28nm for target resist line CD 14nm of low-n attPSM and binary mask with different tonality (DF: dark-field, BF: bright-field).

design polygons can be retargeted, but not easy for the space between these two polygons, due to the vias landing on top. Therefore, the process must print 14nm resist line between these two resist trenches. The middle figure presents the simulated CD vs. the mask space CD of pitch 28nm Two-Bar. The green rectangle is the target 14nm $\pm$ 10% CD variation. Without considering SRAFs, the simulations indicate that only bright-field masks

Downloaded From: https://www.spiedigitallibrary.org/conference-proceedings-of-spie on 19 Sep 2022
Terms of Use: https://www.spiedigitallibrary.org/terms-of-use

can print resist line 14nm on target, and the bright-field low-n attPSM can use slightly larger mask space CD to print the target resist line CD 14nm. The right figure is the measured EL vs. DoF of bright-field masks of low-n attPSM and binary mask for target resist line CD 14nm with ± 10% CD variation. The EL and DoF of the bright-field low-n attPSM are improved by ∼ 40% with respect to the binary bright-field mask.

To enable dark-field mask for printing target resist line CD 14nm, SRAFs insertion is considered. Figure 11 shows the simulated CD vs. the space CD of pitch 28nm Two-Bar without and with 8nm SRAFs. The positions of SRAFs are shown in the left figure. By inserting SRAFs, both dark-field masks of low-n attPSM and the binary mask are able to print the target resist line CD 14nm with the mask space CD 11nm.

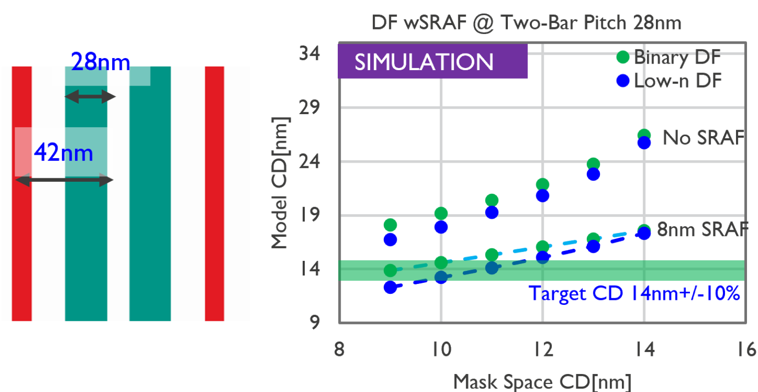

Figure 11: Simulated CD vs. the mask space CD of pitch 28nm Two-Bar without and with 8nm SRAFs (DF: dark-field).

b) Two-Bar Through Slit

Figure 12 compares M3D effects impact on the CD difference through slit using vertical Two-Bar pitch 40nm CD 20nm. The left figure presents the simulated left bar and right bar CD difference. Both dark-field and bright-field binary masks show similar small CD difference through slit. The bright-field low-n attPSM has similar CD difference with an opposite trend through slit with respect to the binary masks. However, the dark-field low-n attPSM delivers a larger CD difference through slit. The middle and right figures in Fig. 12 shows the intensity profile at the left and right edge of the slit for both dark-field and bright-field low-n attPSM of the Two-Bar. The low-n attPSM dark-field mask introduces pronounced intensity imbalance at the edge of the slit with respect to the bright-field mask, which results in the larger CD difference. Therefore, through slit aware OPC is important for dark-field low-n attPSM.

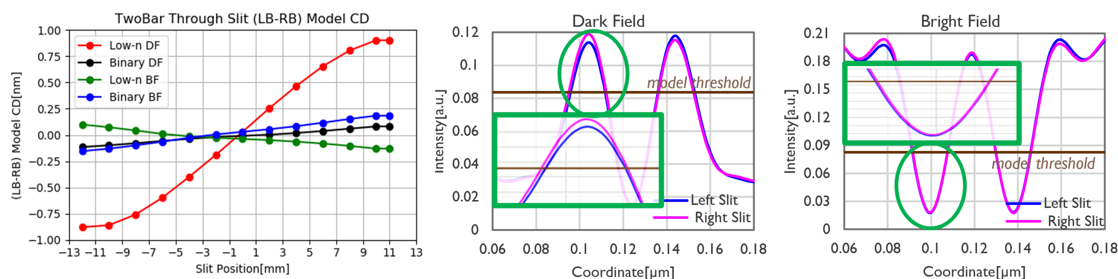

Figure 12: The comparison of pitch 40nm vertical Two-Bar through slit impact (left), and the intensity profile at the left and right edge of the slit for both dark-field and bright-field of low-n attPSM (DF: dark-field, BF: bright-field).

Downloaded From: https://www.spiedigitallibrary.org/conference-proceedings-of-spie on 19 Sep 2022
Terms of Use: https://www.spiedigitallibrary.org/terms-of-use

To have a better understanding of such effects through slit, Fig. 13 shows the schematic of the incident light direction of the Two-Bar at left and right edge of the slit for both dark-field and bright-field masks. The

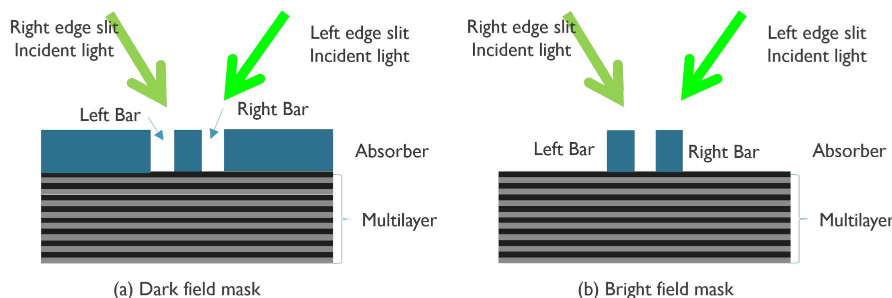

Figure 13: The schematics of the incident light of the Two-Bar at the left slit and right slit

Ta-based absorber binary mask has reflectivity ∼2%, and the low-n attPSM absorber has reflectivity in the range of 8% and 15%.[20] Considering the dark-field masks (cf. Fig. 13(a)) and the Two-Bar placed at the left slit edge. The light incident on the left bar is partly blocked by the thin absorber extension (in x-axis) between these two bars, and of the right bar is partly stopped by the thick absorber extension (in x-axis) on the right side. Due to the thin absorber extension (in x-axis) between these two bars and the high reflectivity of the low-n absorber, the left bar of the dark-field low-n attPSM results in more amount of the reflective light than the right bar, see Fig.12 middle plot. The Two-Bar on the right slit edge shows the opposite. For the bright-field mask (cf. Fig. 13(b)), the two bars get similar amount of the light, the M3D effects are less pronounced (see Fig. 12 right plot).

3.3 T2T Printability

The imec N3 pitch 28nm metal design rule allows aggressive T2T design, the minimum T2T CD is 20nm. Figure 14 shows the simulated and experimental T2T printability at pitch 28nm of low-n attPSMs and binary masks with respect to different mask tonality using the sources in Fig. 1, which are not optimized to print this tight T2T. The simulation results show that to print the target T2T CD of 20nm , the mask T2T CD of the dark-field

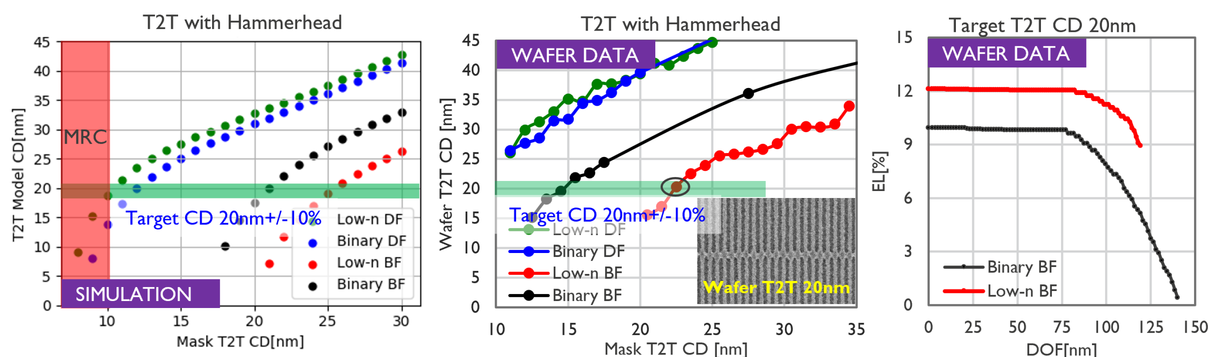

Figure 14: T2T printability at pitch 28nm of low-n attPSM and binary mask with different tonality (DF: dark-field, BF: bright-field).

mask (both low-n attPSM and binary mask) needs to be around 10nm, while of the bright-field low-n attPSM and binary mask needs to be around 20nm and 25nm, respectively. The wafer data in the middle figure shows dark-field masks can not print T2T CD with 20nm on wafer, due to a large T2T pull back vs. the aerial image simulation results. Instead, the bright-field masks can print target T2T CD 20nm. The right figure displays the measured EL vs. DoF for printing target T2T CD 20nm with ± 10% CD variation. The bright-field low-n attPSM improves the EL ∼ 20% with respect to the binary bright-field mask. Figure 14 demonstrates that

Downloaded From: https://www.spiedigitallibrary.org/conference-proceedings-of-spie on 19 Sep 2022
Terms of Use: https://www.spiedigitallibrary.org/terms-of-use

bright-field low-n attPSM delivers the best performance for T2T printing, which enables large mask T2T CD to print smaller target T2T CD on the wafer with higher EL. This is good for OPC.

3.4 Side-lobe Printing

Since the low-n attPSM has a higher reflectivity than the Ta-based binary mask, the slide-lobe printing risk of applying low-n attPSM must be evaluated. Figure 15 shows the aerial image intensity profile distribution at the edge of pitch 28nm Line/Space building block. The model threshold for each case is determined during the MO flow based on the design clip shown in Fig. 2. The left results of bright-field masks in Fig. 15 indicate that the

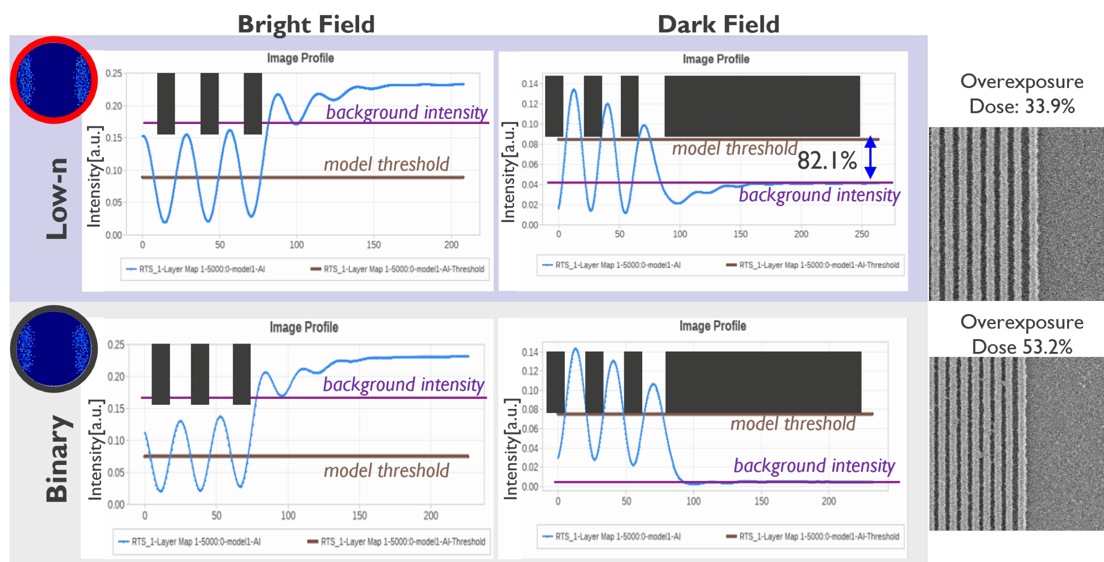

Figure 15: Aerial image intensity profile distribution at the edge of pitch 28nm Line/Space building block at nominal condition, and the measured SEM images of dark-field low-n attPSM with 33.9% and 53.2% overexposure dose respectively.

minimum background intensity of bright-field masks is larger than the maximum intensity of the pitch 28nm Line/Space pattern. Lower the exposure dose will increase the side-lobe printing risk, however, the main features will stop printing earlier. In other word, there is no side-lobe printing issue for bright-field masks. For the dark-field case, Fig. 15 shows the background intensity of the reference binary mask is zero, and we don't have the side-lobe printing issue. However, the background intensity of the low-n attPSM is between the minimum and maximum intensity of the pitch 28nm Line/Space pattern, which means the dark-field low-n attPSM has the risk to print side-lobe. The simulation shows that 82.1% overexposure dose is needed to get the background intensity touch the model threshold. The measured SEM images on the right side of the figure show that it is hard to see the side-lobe print at 33.9% overexposure dose, and could see some speckles at 53.2% overexposure dose while the main features start merging. Therefore, there is no side-lobe printing risk of dark-field low-n attPSM within the OPW for patterning metal layers.

4. SUMMARY

In this paper, the patterning performance of low-n attPSMs and binary masks is compared through simulations and experiments with optimized sources. The impact of mask stack and tonality on the best focus shift through pitch, Two-Bar through slit, the capability of printing Two-Bar and target T2T CD 20nm at pitch 28nm, as well as the side-lobe printing risk is evaluated. The comparative Table 1 summarizes the improvement of each metric when using these two mask candidates.

To apply the dark-field low-n attPSM for patterning pitch 28nm metal design, the mitigation of the large best focus shift through pitch requires design retargting and SRAFs insertion during OPC. However, the dark-field

Downloaded From: https://www.spiedigitallibrary.org/conference-proceedings-of-spie on 19 Sep 2022
Terms of Use: https://www.spiedigitallibrary.org/terms-of-use

Table 1: Comparative summary table of the improvement when using low-n attPSM and binary mask

	Low-n		Binary	
	Dark Field	Bright Field	Dark Field	Bright Field
Best Focus Shift	Large	Small	Small	Small
Need SRAF	Yes (printing risk)	No	No	No
iN3 P28 relevant design NILS	Medium	High	Medium	High
P28 TwoBar targets 14nm Resist Line	Yes (+SRAF)	Yes	Yes (+SRAF)	Yes
M3D effects through slit (Two-Bar)	Pronounced	No	No	No
P28 T2T Targets 20nm	Aggressive MRC	Yes	Aggressive MRC	Yes
Side-lobe Print	No	No	No	No

low-n attPSM has a potential SRAF printing risk (or requires more aggressive MRC). Therefore, SRAF insertion becomes very challenging. Notably, both dark-field low-n attPSM and binary masks could not print target 20nm T2T at pitch 28nm with the current sources, and SRAF insertion is necessary for patterning pitch 28nm Two-Bar with 14nm resist line in the middle. In general, the dark-field low-n attPSM has slightly worse performance with respect to the reference dark-field binary mask.

Compared to the dark-field low-n attPSM, the bright-field low-n attPSM has smaller best focus shift through pitch and higher NILS for pitch 28nm relevent design. SRAFs are not needed to print 14nm resist line in the middle of pitch 28nm Two-Bar. Moreover, bright-field low-n attPSM can print target T2T CD 20nm with large mask T2T CD. With respect to the bright-field binary mask, the bright-field low-n attPSM delivers better patterning performance of Two-Bar and T2T CD 20nm at pitch 28nm. In general, the bright-field low-n attPSM has the best patterning performance with respect to the other three cases.

The imec N3 random logic design clips shown in Fig. 2 with different OPCs have been placed on the low-n attPSM. Further work will focus on the assessment the patterning performance of low-n attPSM using these design clips. Moreover, the current optimized source of the bright-field low-n attPSM in this paper is only using pitch 28nm Line/Space grating as the input target. Adding T2T clips in the SMO to improve the printability of T2Ts and adding Two-Bar clips in SMO to increase the DoF and reduce the best focus shift through pitch will be evaluated.

ACKNOWLEDGMENTS

The authors would like to acknowledge the contributors at imec: Tatiana Kovalevich, Lieve van Look, David Rio (ASML), Max Delorme(ASML)

REFERENCES

[1] Xu, D., Gillijns, W., Drissi, Y., Tan, L. E., Oak, A., and han Kim, R., "EUV single patterning exploration for pitch 28 nm," in [*Design-Process-Technology Co-optimization XV*], Yuan, C.-M. and Kim, R.-H., eds., **11614**, 125 – 136, International Society for Optics and Photonics, SPIE (2021).

Downloaded From: https://www.spiedigitallibrary.org/conference-proceedings-of-spie on 19 Sep 2022
Terms of Use: https://www.spiedigitallibrary.org/terms-of-use

[2] Rio, D., Adrichem, P. V., Delorme, M., Lyakhova, K., Spence, C., and Franke, J.-H., "Extending 0.33 NA EUVL to 28 nm pitch using alternative mask and controlled aberrations," in [*Extreme Ultraviolet (EUV) Lithography XII*], Felix, N. M. and Lio, A., eds., **11609**, 63 – 78, International Society for Optics and Photonics, SPIE (2021).

[3] Franke, J.-H., Frommhold, A., Davydova, N., Aubert, R., Nair, V. V., Kovalevich, T., Rio, D., Bekaert, J., Wang, E., Rispens, G., Maslow, M., and Hendrickx, E., "Metal layer single EUV expose at pitch 28 nm: how bright field and NTD resist advantages align," in [*Extreme Ultraviolet (EUV) Lithography XII*], Felix, N. M. and Lio, A., eds., **11609**, 43 – 62, International Society for Optics and Photonics, SPIE (2021).

[4] Simone, D. D., Kljucar, L., Das, P., Blanc, R., Beral, C., Severi, J., Vandenbroeck, N., Foubert, P., Charley, A., Oak, A., Xu, D., Gillijns, W., Mitard, J., Tokei, Z., van der Veen, M., Heylen, N., Teugels, L., Le, Q. T., Schleicher, F., Leray, P., Ronse, K., Kim, I. H., Kim, I., Park, C., Lee, J., Ryu, K., Schepper, P. D., Doise, J., and Kocsis, M., "28nm pitch single exposure patterning readiness by metal oxide resist on 0.33NA EUV lithography," in [*Extreme Ultraviolet (EUV) Lithography XII*], Felix, N. M. and Lio, A., eds., **11609**, 43 – 53, International Society for Optics and Photonics, SPIE (2021).

[5] Erdmann, A., Evanschitzky, P., Neumann, J. T., and Graeupner, P., "Mask-induced best-focus shifts in deep ultraviolet and extreme ultraviolet lithography," *Journal of Micro/Nanolithography, MEMS, and MOEMS* **15**, 1–11 (2016).

[6] Erdmann, A., Xu, D., Evanschitzky, P., Philipsen, V., Luong, V., and Hendrickx, E., "Characterization and mitigation of 3D mask effects in extreme ultraviolet lithography," *Adv. Opt. Techn.* **6**, 187–201 (2017).

[7] Philipsen, V., Luong, K. V., Souriau, L., Hendrickx, E., Erdmann, A., Xu, D., Evanschitzky, P., van de Kruijs, R. W. E., Edrisi, A., Scholze, F., Laubis, C., Irmscher, M., Naasz, S., and Reuter, C., "Reducing EUV mask 3D effects by alternative metal absorbers," **10143**, 174 – 188 (2017).

[8] Franke, J.-H., Bekaert, J., Blanco, V., Look, L. V., Wahlisch, F., Lyakhova, K., van Adrichem, P., Maslow, M. J., Schiffelers, G., and Hendrickx, E., "Improving exposure latitudes and aligning best focus through pitch by curing M3D phase effects with controlled aberrations," in [*International Conference on Extreme Ultraviolet Lithography 2019*], Itani, T., Gargini, P. A., Naulleau, P. P., and Ronse, K. G., eds., **11147**, 50 – 69, International Society for Optics and Photonics, SPIE (2019).

[9] Burkhardt, M., "Investigation of alternate mask absorbers in EUV lithography," in [*Extreme Ultraviolet (EUV) Lithography VIII*], Panning, E. M., ed., **10143**, 195 – 208, International Society for Optics and Photonics, SPIE (2017).

[10] Philipsen, V., Luong, K. V., Opsomer, K., Detavernier, C., Hendrickx, E., Erdmann, A., Evanschitzky, P., van de Kruijs, R. W. E., Heidarnia-Fathabad, Z., Scholze, F., and Laubis, C., "Novel EUV mask absorber evaluation in support of next-generation EUV imaging," in [*Photomask Technology 2018*], Gallagher, E. E. and Rankin, J. H., eds., **10810**, 53 – 65, International Society for Optics and Photonics, SPIE (2018).

[11] Finders, J., de Kruif, R., Timmermans, F., Santaclara, J. G., Connely, B., Bender, M., Schurack, F., Onoue, T., Ikebe, Y., and Farrar, D., "Experimental investigation of a high-k reticle absorber system for EUV lithography," in [*Extreme Ultraviolet (EUV) Lithography X*], Goldberg, K. A., ed., **10957**, 268 – 276, International Society for Optics and Photonics, SPIE (2019).

[12] Sejpal, R., Philipsen, V., Armeanu, A., Wei, C.-I., Gillijns, W., Lafferty, N., Fenger, G., and Hendrickx, E., "Exploring alternative EUV mask absorber for iN5 self-aligned block and contact layers," in [*Photomask Technology 2019*], Rankin, J. H. and Preil, M. E., eds., **11148**, 265 – 276, International Society for Optics and Photonics, SPIE (2019).

[13] Erdmann, A., Mesilhy, H. S., Evanschitzky, P., Philipsen, V., Timmermans, F. J., and Bauer, M., "Perspectives and tradeoffs of absorber materials for high NA EUV lithography," *Journal of Micro/Nanolithography, MEMS, and MOEMS* **19**(4), 1 – 16 (2020).

[14] Philipsen, V., "Mask is key to unlock full EUVL potential," in [*Extreme Ultraviolet (EUV) Lithography XII*], Felix, N. M. and Lio, A., eds., **11609**, International Society for Optics and Photonics, SPIE (2021).

[15] Wu, M., Thakare, D., de Marneffe, J.-F., Jaenen, P., Souriau, L., Opsomer, K., Soulié, J.-P., Erdmann, A., Mesilhy, H. M. S., Naujok, P., Foltin, M., Soltwisch, V., Saadeh, Q., and Philipsen, V., "Study of novel EUVL mask absorber candidates," *Journal of Micro/Nanopatterning, Materials, and Metrology* **20**(2), 1 – 13 (2021).

Downloaded From: https://www.spiedigitallibrary.org/conference-proceedings-of-spie on 19 Sep 2022
Terms of Use: https://www.spiedigitallibrary.org/terms-of-use

[16] Xu, D., Gillijns, W., Tan, L. E., Philipsen, V., and han Kim, R., "Exploration of alternative mask for 0.33NA EUV single patterning at pitch 28nm ," in [*International Conference on Extreme Ultraviolet Lithography 2021*], Ronse, K. G., Naulleau, P. P., Gargini, P. A., Itani, T., and Hendrickx, E., eds., **11854**, 69 – 81, International Society for Optics and Photonics, SPIE (2021).

[17] Xu, D., Gillijns, W., Tan, L. E., Philipsen, V., and Kim, R.-H., "Exploration of alternative mask for 0.33NA extreme ultraviolet single patterning at pitch 28-nm metal design," *Journal of Micro/Nanopatterning, Materials, and Metrology* **21**(2), 1 – 15 (2022).

[18] Erdmann, A., Evanschitzky, P., Mesilhy, H., Philipsen, V., Hendrickx, E., and Bauer, M., "Attenuated PSM for EUV: Can they mitigate 3D mask effects?," in [*Extreme Ultraviolet (EUV) Lithography IX*], Goldberg, K. A., ed., **10583**, 258 – 270, International Society for Optics and Photonics, SPIE (2018).

[19] van Lare, M.-C., Timmermans, F. J., and Finders, J., "Alternative reticles for low-k1 EUV imaging," in [*International Conference on Extreme Ultraviolet Lithography 2019*], Itani, T., Gargini, P. A., Naulleau, P. P., and Ronse, K. G., eds., **11147**, 39 – 49, International Society for Optics and Photonics, SPIE (2019).

[20] van Lare, C., Timmermans, F., Finders, J., Romanets, O., Man, C.-W., van Adrichem, P., Ikebe, Y., Aizawa, T., and Onoue, T., "Investigation into a prototype extreme ultraviolet low-n attenuated phase-shift mask," *Journal of Micro/Nanopatterning, Materials, and Metrology* **20**(2), 1 – 11 (2021).

[21] van de Kerkhof, M., Jasper, H., Levasier, L., Peeters, R., van Es, R., Bosker, J.-W., Zdravkov, A., Lenderink, E., Evangelista, F., Broman, P., Bilski, B., and Last, T., "Enabling sub-10nm node lithography: presenting the NXE:3400B EUV scanner," in [*Extreme Ultraviolet (EUV) Lithography VIII*], Panning, E. M., ed., **10143**, 34 – 47, International Society for Optics and Photonics, SPIE (2017).

Downloaded From: https://www.spiedigitallibrary.org/conference-proceedings-of-spie on 19 Sep 2022
Terms of Use: https://www.spiedigitallibrary.org/terms-of-use